MATCHED SUBSPACE DETECTORS FOR DISCRIMINATION OF TARGETS FROM TREES IN SAR IMAGERY

A. Sharma and R. L. Moses

Department of Electrical Engineering
The Ohio State University
Columbus, OH 43210 USA

ABSTRACT

We investigate the use of subspace-based detectors for discriminating vehicles from trees in low frequency synthetic aperture imagery. We model tree scattering as structured isotropic interference responses and model dominant vehicle scattering as dihedral responses. We form linear subspaces of tree and target responses, and apply subspace-based detection methods developed by Scharf and Friedlander. Analysis on synthetic tree and target models show the viability of this approach. Preliminary results on measured imagery provide lower performance, suggesting the need for improved data calibration and improved scattering models of trees at low frequencies.

1. INTRODUCTION

Constant False Alarm Rate (CFAR) detectors are often employed for object detection in radar imagery. CFAR detectors attempt to find points of interest whose amplitude or energy is large in comparison to scattered energy in the neighborhood of the point. A two-parameter Gaussian CFAR detector is often used, in which one assumes the clutter statistics to be Gaussian with unknown mean and variance.

CFAR detectors often give unacceptably high false alarm rates in forested areas for a desired probability of detection. For low-frequency radar imagery, one reason is that forest clutter is often not well modeled as Gaussian noise; tree trunk scattering appears as a locally bright region and passes the CFAR detection test. CFAR detectors have been developed that employ a heavy-tailed clutter distribution, such as the K-distribution or an α-stable random process [2, 3]; these methods give some improvement, but still yield high false alarm rates.

Prepared through collaborative participation in the Advanced Sensors Consortium sponsored by the U.S. Army Research Laboratory under the Federated Laboratory Program, Cooperative Agreement DAAL01-96-2-0001. The U.S. Government is authorized to reproduce and distribute reprints for Government purposes notwithstanding any copyright notation thereon.

Several approaches that exploit forest clutter structure have been proposed for target detection in FOPEN-SAR environments. Many of these techniques make use of the radar's angle diversity to discriminate between target and tree responses. Allen and Hoff [4] demonstrated the use of a physics based model for both targets and trees, and used a matched filter detector to reduce the number of false alarms. Chaney *et.al.* [5] proposed an adaptive image formation procedure in order to enhance man-made scatterers in FOPEN-SAR images. Kim *et.al.* [6] apply a non-parametric density estimator to characterize the behavior of data using distributions of signal energy over subapertures at different resolutions, and then use these densities for discrimination of target, tree, and clutter classes. Marble and Gorman [7] use phenomenology based features derived from scattering physics predictions combined in a quadratic classifier to discriminate between targets and trees. Finally, Nguyen *et.al.* [8] fit ellipsoid templates to differentiate between tree clutter and target responses.

In this paper we consider a hypothesis testing approach to the object detection problem, treating tree scattering as a structured interference component. We assume that the radar signal is a combination of objects of interest, of background clutter modeled as random noise, and of a structured interference term of unknown amplitude to model tree scattering. We model the structure in the interference as a low-dimensional linear subspace which we determine using principal components analysis. In a similar way, targets are also modeled as elements in a linear subspace. By selecting different dimensions and bases of the subspaces, we can encode more or less prior information about targets and interference. Subspace modeling also results in closed-form expressions and analytical expressions for detection performance [1].

2. DETECTION PROBLEM

The detection processing system is shown in Figure 1. A full scene SAR image is first passed through a conventional

0-7803-6514-3/00/$10.00©2000 IEEE

Figure 1: System Model

CFAR prescreener, which identifies subset image regions for further processing. The output of the prescreener stage is a set of point-of-interest (POI) chips, which are generally comprised of tree and target responses. These chips are then passed through an interference rejection stage, which attempts to reduce false alarms due to tree scattering while maintaining a desired detection probability. The output of the interference rejection stage is sent to a target classifier, which performs additional processing on the image chips to classify detected targets. This paper focuses on algorithms for the interference rejection block.

2.1. Signal Model

The input to detector is an $m \times 1$ data vector, $\bar{y}$, which is obtained by stacking the columns of the point-of-interest (POI) image chip obtained from a prescreener. We model this signal vector as

$$\bar{y} = H\bar{\theta} + S\bar{\phi} + \sigma\bar{n} \tag{1}$$

where H is an $m \times p$ matrix whose columns span the desired signal subspace and S is an $m \times t$ matrix whose columns span the interference signal subspace. The matrices H and S encode partial knowledge about the signal and interference, respectively. The vectors $\bar{\theta}$ and $\bar{\phi}$ are the coordinates of the signal and interference components in their respective subspaces. The vector $\bar{n}$ is an $m \times 1$ noise vector, which is modeled as additive, zero mean, white Gaussian noise with unit variance. The noise power is given by σ^2. We assume both H and S are known, while $\bar{\theta}$ and $\bar{\phi}$ are deterministic unknowns. The noise variance σ^2 may be known or unknown.

2.2. Detector Structures

The signal detection problem can be formulated as the following hypothesis testing problem, after [1]:

$$H_0: \quad \bar{y} = S\bar{\phi} + \sigma_0\bar{n} \tag{2}$$

$$H_1: \quad \bar{y} = H\bar{\theta} + S\bar{\phi} + \sigma_1\bar{n} \tag{3}$$

Optimal detectors for this problem are derived in [1]. These detectors estimate the desired signal energy after projecting $\bar{y}$ in a direction orthogonal to the interference subspace, and compare it to the noise energy present in this direction. The test statistic, which is the ratio of these two energies, is then compared to a threshold to make a decision. These detectors have been shown to be UMP among the set of all detectors which have certain desired invariances [1].

We consider two scenarios: the noise variance σ^2 known, and the noise variance σ^2 unknown. For the known variance case, the test statistic is a generalized likelihood ratio given by

$$L_1(\bar{y}) = \frac{1}{\sigma^2}\|P_G P_S^{\perp}\bar{y}\|^2 \tag{4}$$

where, P_G is a projection operator into the subspace $\langle G \rangle$ and $P_S^{\perp}$ is a projection operator projecting orthogonal to the subspace $\langle S \rangle$. The subspace $\langle G \rangle$ represents the subspace where the signal component $H\bar{\theta}$ lies after being operated upon by $P_S^{\perp}$. The likelihood ratio in Equation (4) can be easily seen to be a ratio of two energies. Hence the detector can be viewed as a generalized energy detector, which first projects the input vector orthogonally to the interference subspace, then projects the residual ($P_S^{\perp}\bar{y}$) onto the signal subspace and compare the energy of this final residual ($P_G(P_S^{\perp}\bar{y})$) with the known noise power.

For the unknown variance case, the test statistic is given by

$$L_2(\bar{y}) = \frac{\|P_G P_S^{\perp}\bar{y}\|^2}{\|P_G^{\perp} P_S^{\perp}\bar{y}\|^2} \tag{5}$$

Again, we can see that the test statistic is a ratio of two quadratic forms. In this case, the numerator term is the same as that in Equation (4). The denominator term represents the estimated noise power, obtained by projecting the input signal orthogonal to both the desired signal and the interference subspaces ($P_G^{\perp}(P_S^{\perp}\bar{y})$).

The probability distributions of the test statistics are mono tone as a function of the signal-to-noise ratio (SNR), and the corresponding detectors are UMP [1].

3. PERFORMANCE ANALYSIS

Experiments from measured FOPEN-SAR data [4, 5, 6, 7] suggest a property which can be used for distinguishing between the target and interference classes at low frequencies. Trees are modeled as isotropic reflectors because most of the scattered response emanates from the top-hat reflector formed between the tree trunk and ground. Thus, tree trunk responses do not change significantly as a function of aspect angle of the radar. On the other hand, targets often exhibit strong anisotropic responses and are modeled as dihedrals [9].

3.1. Tree Models

We consider two choices for the interference subspace. At one extreme, we consider a one-dimensional approximation of a tree response as predicted from the geometric theory of

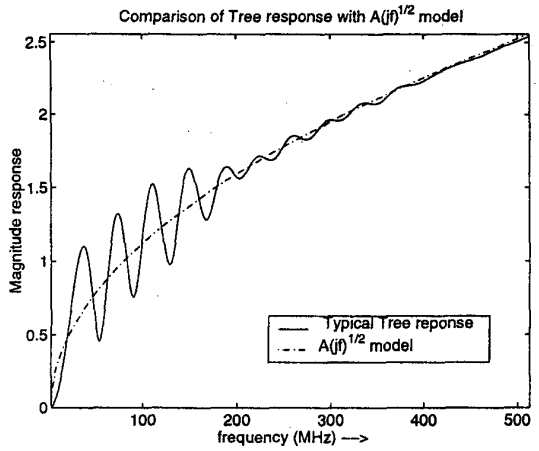

Figure 2: Comparison of FDTD-model response with $A(jf)^{1/2}$ response

diffraction (GTD). The GTD tree response in the frequency-aspect domain (f, θ) is given by [12]

$$T(f, \theta) = A(jf)^{\frac{1}{2}} \tag{6}$$

Here, A is the amplitude and θ is the aspect angle at which the radar views the tree with respect to broadside. The response is isotropic (*i.e.,* it does not depend on θ). The interference subspace, $\langle S \rangle$, consists of a tree image generated by using Equation (6). For an arbitrary, amplitude A, the response lies in a one-dimensional subspace ($t = 1$).

The GTD approximation (6) has been compared to a more elaborate Finite Difference Time Domain (FDTD) scattering prediction model of a tree trunk response [11]. Figure 2 shows that the model provides a good fit to the FDTD response (the mean square error value for the above fit is 1.4%). The oscillatory behavior of the FDTD prediction at low frequencies is largely due to scattering from the top of the truncated tree trunk model — the model tree is truncated to a height of 7 m for computational reasons. Thus, this oscillatory behavior is not characteristic of field measurements.

The second interference subspace we consider is an isotropic basis model. We choose a set of basis vectors that spans the space of all isotropic responses which are time-limited (in a user-specified time-interval) and also nearly bandwidth-limited to the radar system bandwidth. The subspace dimension is given by the time-bandwidth product and is $t \approx 20$ for this application [11]. These basis vectors are transformed into images using an image simulator [10] and used as the basis set for the isotropic interference subspace.

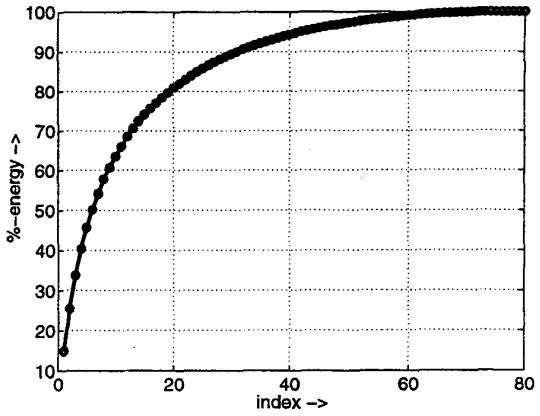

Figure 3: Cumulative percent energy in principal singular values from dihedral training set images chips.

3.2. Target Model

The signal subspace, $\langle H \rangle$ is modeled by the set of dihedral responses. The frequency response of a dihedral is given by [9]

$$S(f, \theta) = A_0 \frac{2\pi f}{c} \operatorname{sinc}\left(\frac{2\pi f}{c} L \sin(\theta - \theta_0)\right) \tag{7}$$

where θ_0 is the orientation of the dihedral with respect to broadside and L is the dihedral length.

The set of dihedral responses form a two-dimensional nonlinear manifold in $\mathcal{R}^m$ parameterized by (L, θ_0). We approximate this two-dimensional nonlinear manifold with a p-dimensional linear subspace. This is done by sampling the non-linear manifold at several points of (L, θ_0), performing a principal component analysis of the sampled set, and selecting the singular vectors corresponding to the p largest singular values. As an example, Figure 3.2 shows the percent energy captured in the first p singular values for dihedrals with lengths $0 \leq L \leq 2$ m and orientations $-45° \leq \theta_0 \leq 45°$, for a UWB radar system [11].

3.3. Effect of Image Shifts

The above tree and target models assume perfect knowledge of the location of a scattering object. In practice these locations are not known, but can be estimated to within 1-2 pixels. The subspace detectors can be made robust to location uncertainty by including shifted versions of tree and dihedral scattering vectors in forming the respective subspaces. Subspace designs for ± 2 pixel shifts are developed in [11] and shown to be effective; for the cases considered, the subspace dimensions increased by approximately 60%.

3.4. Performance Analysis

In this subsection we analyze detection performance for the tree and target subspaces modeled in Sections 3.1 and 3.2. We use a 2 m×2 m image chip, which has $m = 1045$ pixels, and consider two interference subspace models, the GTD tree model with $dim(\langle S \rangle) = t = 1$ and the generalized isotropic interference model with $dim(\langle S \rangle) = t = 20$. For each case we consider two target subspace dimensions, $p = 10$ and $p = 55$, which from Figure 3 models about 60% or 95% of dihedral scattering energy. Detection performance results are obtained using the analytical expressions presented in [1].

Figure 3.4 presents ROC curves showing P_d versus P_{fa}. For each case, both the known noise variance and unknown noise variance detector performance is shown, and the target SNR = 20dB. These results show good detection performance at low P_{fa} (~ 0.1), which suggests that they are capable of reducing false-alarms while maintaining good detection performance.

4. EXPERIMENTS ON MEASURED DATA

We have applied the subspace-based detection procedure to measured UWB radar imagery containing trucks located in a forested region. The radar has an operating frequency range of 200-1300 Mhz and images are formed from an aspect aperture of approximately 90° [8]. Imagery is formed using a backprojection algorithm. Importantly, no calibration for nonideal antenna characteristics is implemented yet, so frequency and aspect variations of the antennas are included in the imagery. In particular, the image of an isotropic scattering object appears as anisotropic due to nonideal antenna responses.

We have applied the subspace processing method using several sources from which to develop an interference subspace. First, both the GTD model and the isotropic subspace model in Section 3.1 is used. Second, a small number of power poles in the scene were used as "ideal" tree trunk responses, and used to form the interference subspace. Finally, a set of measured images of trees in the scene were used.

Performance of the resulting detectors, when applied to the measured SAR imagery, was significantly lower than predicted by synthetic data experiments. The main reason is the inadequate modeling of the interference component in the test vectors by a low-dimensional subspace. Figure 4 shows an example of the modeling. In the figure, we use power poles to construct an interference subspace, and plot the fractional residual norm metric $\xi(\bar{y}) = \frac{\|P_S^{\perp} \bar{y}\|}{\|\bar{y}\|}$ as a function of subspace dimension. In the figure we plot the fractional residual norm of four data sets: the power poles (used to generate the subspace), vehicles in the scene, trees in the scene, and synthetic ideal dihedral response image chips.

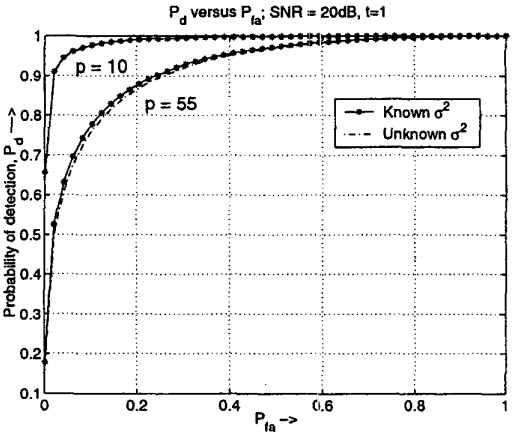

(a) $\dim(\langle S \rangle) = t = 1$

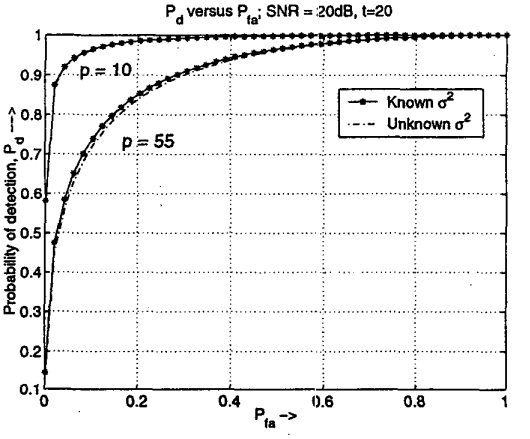

(b) $\dim(\langle S \rangle) = t = 20$

Figure 4: ROC curves for dihedral detection in the presence of tree interference.

We see that the residual fractional norm of the power poles decreases with increasing subspace dimension, with 30% fractional norm remaining (meaning more than 90% of energy modeled) for $p \geq 76$. On the other hand, trees showed a markedly higher residual norm, and the residual norm of trees and vehicles show no difference. Experiments with other interference subspaces [11] give similar results.

There are two hypothesized reasons for the relatively poor modeling of the tree scattering in a low-dimensional subspace. One possible reason is that available imagery is not calibrated to remove antenna frequency and aspect responses. We attempted a simple calibration procedure to remove some effects of nonideal antenna responses, using the average magnitude of the frequency-aspect response of power poles. No phase calibration was attempted. This sim-

ple calibration procedure is known to have limitations; in particular, it is known that the required calibration is spatially-variant [10]. It is likely that this simple calibration is not adequate for good performance of the detectors, because the detectors are based on the assumption that tree scattering is isotropic. Improved antenna calibration of the imagery is a topic of current research, so testing of the subspace-based detection method on well-calibrated data should be possible in the near future.

A second possible reason for poor performance is that scattering responses from trees in the scene are not well-modeled as isotropic scattering responses. Most trees in the scene are deciduous, and many have large branches that spread from the main trunk. Little published work (either analytical or empirical) has appeared on characterizing tree responses at low frequencies; analytical work to date has focused on tree trunk models, and empirical analysis has been limited by a relatively small amount of measured data at low frequencies and high resolution. Further work is needed to understand whether each of these hypothesized reasons for performance limitation are correct, and what relative impact each has on overall performance.

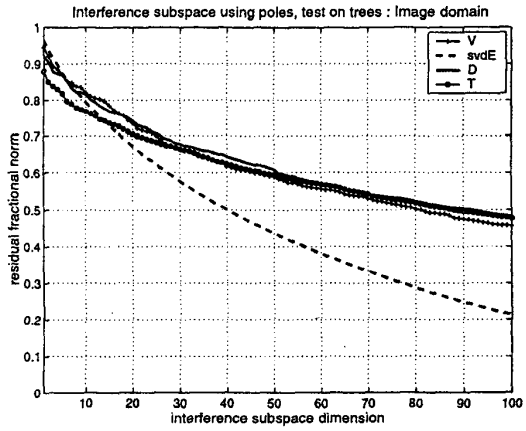

Figure 5: Residual fractional norm of scattering responses when projected orthogonally to an interference subspace formed from power poles. Shown are residual norms for vehicle chips (V), synthetic dihedral chips (D), tree chips (T), and power pole chips (svdE).

5. CONCLUSION

We investigated the problem of detecting vehicles in forested regions from low frequency, ultra-wideband radar imagery. We proposed the use of subspace-based detectors to discriminate image chips containing vehicles from those containing trees. We consider a detection problem with interference terms, where the interference represents scattering due to trees. We exploit the property that tree trunk responses, which are expected to dominate the backscattered energy from trees, are isotropic, whereas vehicle responses have strongly anisotropic dihedral-like characteristics. We model the tree and target responses elements of linear subspaces, and form the subspace basis vectors using models of isotropic tophat scattering centers, general isotropic scattering centers, and dihedrals.

Analysis of synthetic data showed that both tree and target subspaces are well-modeled as subspaces of low dimension, and that these subspaces are separated enough to provide desired detection performance at reasonable target signal-to-noise ratios. Detection performance was significantly worse when the detectors were applied to measured data. Two hypothesized reasons for the performance drop are 1) inadequate image calibration for effective use of these detectors, and 2) tree scattering is not well-modeled as an isotropic tree-trunk response. Current research aimed at improved data calibration and improved tree modeling should provide further insight and evidence to test these hypotheses.

6. REFERENCES

[1] L. L. Scharf and B. Friedlander, "Matched subspace detectors," *IEEE Transactions on Signal Processing*, vol. 42, pp. 2146–2157, August 1994.

[2] A. Banerjee, P. Burlina, and R. Chellappa, "Adaptive target detection in foliage-penetrating SAR images using alpha-stable models," in *Algorithms for Synthetic Aperture Radar Imagery*, September 1997.

[3] R. L. Dilsavor and R. L. Moses, "Fully polarimetric GLRT for detecting targets with unknown amplitude, phase, and tilt angle in terrain clutter," in *Proc. SPIE International Symposium on Automatic Target Recognition IV*, vol. 2234, (Orlando, FL), pp. 14–25, April 1994.

[4] M. R. Allen, J. M. Jauregui, and L. E. Hoff, "FOPEN-SAR detection by direct use of simple scattering physics," in *Proceedings of the SPIE International symposium on Algorithms for Synthetic Aperture Radar imagery II* (D.A.Giglio, ed.), vol. 2487, (Orlando,FL), pp. 45–55, April 1995.

[5] R. D. Chaney, A. S. Wilsky, and L. M. Novak, "Coherent aspect-dependent SAR image formation," in *Proceedings of the SPIE, Algorithms for SAR imagery*, vol. 2234, pp. 256–274, April 1994.

[6] A. Kim, J. Fisher, A. Willsky, and P. Viola, "Nonparametric estimation of aspect dependance for ATR," in *Algorithms for Synthetic Aperture Radar Imagery VI*, (Orlando, FL), pp. 332–342, SPIE, April 1999.

[7] J. A. Marble and J. D. Gorman, "Performance comparison of phenomenology-based features to generic features for false alarm reduction in UWB SAR imagery," in *Algorithms for Synthetic Aperture Radar Imagery VI*, vol. 3721, (Orlando, FL), pp. 235–242, SPIE, April 1999.

[8] L. Nguyen, R. Kapoor, and J. Sichina, "Detection algorithms for ultra-wideband foliage penetration radar," in *Proceedings of SPIE, Radar Sensor Technology II*, April 1997.

[9] E. Erten, "Performance analysis of anisotropic scattering center detection," Master's thesis, The Ohio State University, 1997.

[10] R. Rajagopal, E. Ertin, and L. C. Potter, "Data simulation and image quality evaluation for fully polarimetric wideband wide-angle radar," in *Third Annual ARL Federated Laboratory Symposium*, (College Park, MD), February 1-5 1999.

[11] A. Sharma, "Automatic Target Detection in Tree-Scattering Interference," Master's thesis, The Ohio State University, 2000.

[12] A. A. Nowotarski, "Electromagnetic scattering from the trunks and branches of trees," Master's thesis, The Ohio State university, 1993.